A New Technique for Measuring Isotopic Impurity Diffusion in Solid Helium

D. Hanneke

Physics Department, Case Western Reserve University, Cleveland, Ohio 44106

The diffusion of isotopic impurities in solid ^{4}He is an excellent probe for determining the properties of vacancy waves. Reported coefficients for diffusion via vacancies and the temperature dependencies of these coefficients are at variance with each other and may result from an anisotropic diffusion tensor. We have proposed a new technique for observing this behavior using an rf reflection spectrometer at a fixed frequency and three orthogonal gradient coils. We have designed and built an apparatus to test our technique, and it is nearly operational.

INTRODUCTION

Helium crystallizes only at high pressure. Even at the absolute zero of temperature, its quantum mechanical zero-point energy produces vibrations that prevent crystallization below roughly 25 atm (2.5 MPa), as can be seen in its phase diagram (Figure 1). When it does solidify, it forms simple structures (hcp, bcc, fcc) of high regularity; solid helium maintains its periodicity over large distances and single crystals are easy to grow.[1] Helium can be described as a quantum solid because the zero-point motion of the atoms is a significant fraction of the nearest neighbor distance.[2] The first prediction of a macroscopic effect of a quantum solid was made by Andreev and Lifshitz[3] and concerned defects in the crystals.

In a quantum solid, it is difficult to localize atoms to lattice sites. Their wavefunctions overlap, raising the possibility of exchange. If there is a defect in a crystal (e.g. a different isotope or atom or a vacancy), it too is non-localized and can exchange. While the switching of two identical lattice elements does not change the crystal, an exchange of a lattice element and an impurity does. Solid helium is an ideal quantum solid in which to study the theory of defects because the zero-point motion of atoms is so large that one can treat them like waves (referred to as defectons). One measures the motion of defectons with a diffusion constant, D.

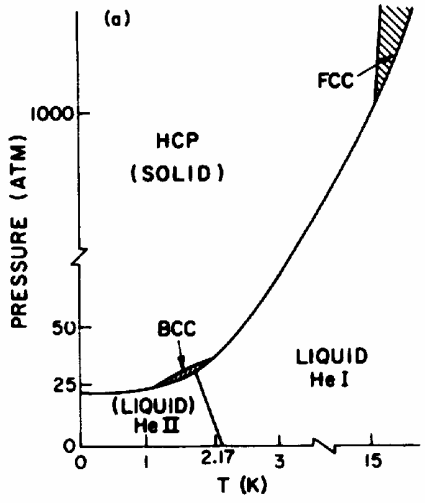

Figure 1: Phase diagram of ^{4}He. From Glyde[2].

The original calculations of the diffusion constant were carried out for ^{3}He impurities in a ^{4}He solid by Andreev and Lifshitz[3], and more detailed results are presented in Allen and Richards[4], Allen *et al*[5], and Grigor'ev[6]. For low ^{3}He concentrations, there are three distinct temperature regions.

At low temperatures, the impurities can be regarded as a gas of quasiparticles that only interact with each other and tunnel through the ^{4}He. The diffusion coefficient can be quantified as

$$D \approx J_{34}\, a^4 / h\, s\, x_3 \qquad (1)$$

where J_{34} is the ^{3}He–^{4}He tunnel rate, a is the lattice spacing, s is the cross section of the ^{3}He–^{3}He interaction, and x_3 is the fraction of ^{3}He. Lengthy estimates of the cross section are presented in Grigor'ev[6] and involve the fact that the ^{3}He impurity has a larger zero-point vibration and thus occupies a larger volume in the lattice. The ^{3}He atoms interact with each other elastically between their distorted regions in the lattice. To within a constant, the diffusion coefficient can be represented as

$$D \propto (J_{34}\, a^2 / x_3)(J_{34} / U_0)^{2/3} \qquad (2)$$

where U_0 is the interaction potential between two ^{3}He atoms at a distance a. It is important to note that D depends on J_{34} but not on temperature in this region.

At higher temperatures, the scattering of the defectons is predominantly by phonons. To within a constant, the diffusion coefficient can be written

$$D \propto \hbar\, J_{34}^2\, a^2\, Q_D^{\,8} / k_B\, T^{\,9} \qquad (3)$$

where Q_D is the Debye temperature for ^{4}He and T is the temperature.

At even higher temperatures, the scattering length (i.e. mean free path) of the impurities is on the order of a lattice spacing, so incoherent diffusion takes over. The diffusion is primarily into vacancies, rather than a ^{3}He–^{4}He exchange. Calculations of D here are based on random walks, and D can be estimated as

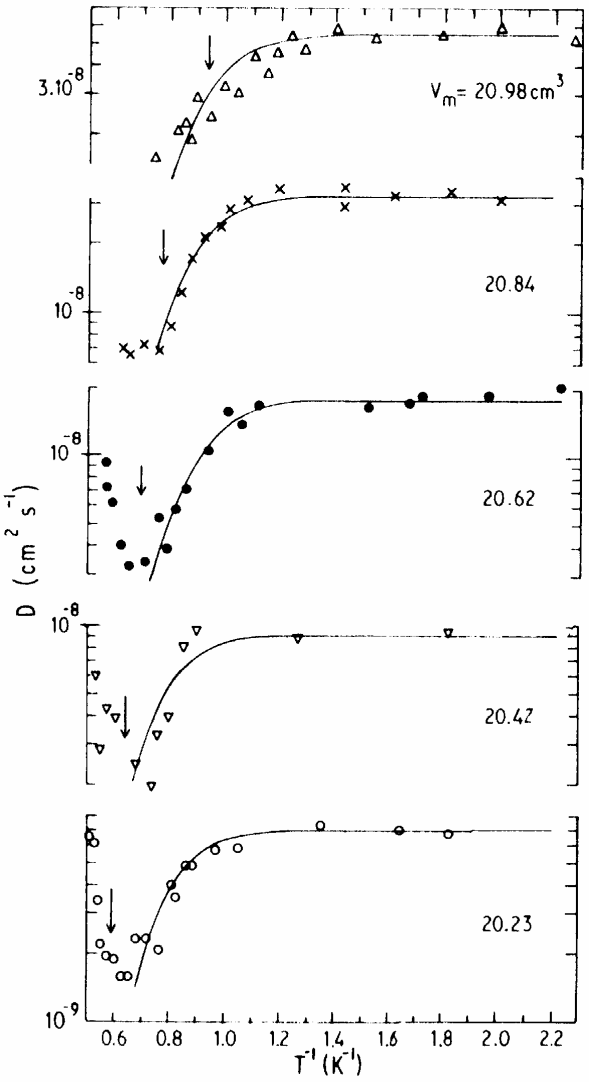

Figure 2: Temperature dependence of the spin diffusion coefficient of ^{3}He of fractional concentration 5 x 10^{-4} in solid ^{4}He for five different labeled molar volumes. From Allen *et al*[5].

$$D \approx D_0 \exp (- W / k_B T) \qquad (4)$$

where W is the activation energy for vacancy formation.

A sample of data verifying these trends is taken from Allen *et al*[5] and is shown in Figure 2. Here, the diffusion constant is plotted against inverse temperature for five different molar volumes of ^{4}He, all with x_3 = 0.05%. (Different molar volumes indicate different pressures, with a higher pressure sample having a lower molar volume.) The three temperature regions are distinct. The first, ^{3}He–^{3}He interaction dominated region has D independent of temperature ($T^{-1} > 1.2$ K^{-1} or $T < 0.8$ K). The second, phonon dominated region has D decreasing as T^{-9} (a positively sloping line, since the plot is logarithmic in D and inverse in T) (1.2 K^{-1} > T^{-1} > 0.67 K^{-1} or 0.8 K < T < 1.5 K). The third, vacancy dominated region shows an increase in the diffusion constant as temperature becomes higher ($T^{-1} < 0.67$ K^{-1} or $T > 1.5$ K). The fitted curves are to the first and second regions (Equations 2 and 3).

It is the vacancy dominated region that motivates the development of a new technique. Published data on the diffusion of ^{3}He impurities in hcp ^{4}He via vacancies are in wide disagreement.[7,8] This diffusion follows Equation 4, and the exponential is associated with the density of vacancies. At a given molar volume (pressure), activation energies vary over a range of a factor of two, and the diffusion coefficient prefactors (D_0) cover a range of two orders of magnitude. These ranges are identical to the corresponding quantities for positive ion diffusion in hcp ^{4}He. Experiments on ion mobilities (such as those described in Lau and Dahm[8], Lau *et al*[9], and Andreeva *et al*[10]) demonstrate that the diffusion coefficient for the positive ion is highly anisotropic with the activation energy for motion in the basal plane equal to twice the corresponding quantity normal to the plane. It has been suggested that two vacancies are required to move an ion in the basal plane.[11] The positive ion grossly distorts the lattice via electrostriction. An isotopic impurity, which creates a much smaller lattice distortion, is a better probe of vacancy waves.

Previous directional diffusion measurements on isotopic impurities in hcp ^{4}He were made on samples assumed to be multi-crystalline. However, helium crystals anneal rapidly, and many of these crystals may have been of unknown orientation. We propose that the diffusion coefficient for isotopic impurities in ^{4}He is given by a tensor with the activation energies and prefactors similar to those for the positive ion. A measurement of a highly anisotropic diffusion tensor for isotopic impurities as well as a tensor that mimics that of the positive ion would alter our present model of vacancy waves. Our experiment is designed to measure the diffusion of ^{3}He nuclear spins in three orthogonal directions on a single hcp ^{4}He crystal and to test this hypothesis.

PREVIOUS EXPERIMENTAL METHODS

The method used to study the diffusion of impurities in solid helium has been pulse nuclear magnetic resonance (NMR). NMR relies on the spin of a particle; in these experiments, it was used to track the motion of ^{3}He, which has a net spin (^{4}He does not). In a static magnetic field in the z-direction, spins will tend to align themselves either parallel or anti-parallel to the field. In NMR, a pulse at the resonant frequency (see Equation 6) is applied perpendicular to the field, which rotates the spins. If it rotates the spins perpendicular to the field, it is called a 90^o (or π/2) pulse; if it flips them over, it is called a 180^o (or π) pulse. After the pulse is applied, the spins will gradually recover to their original parallel states. The

characteristic time this recovery takes is called T_1 and is quantified as

$$M_z(t) = M_0 (1 - \exp(-t / T_1)) \quad (5)$$

where $M_z(t)$ is the net magnetization in the z-direction as a function of time.

When the spins saturate, they precess about the z-axis at the Larmour frequency, which is

$$w_L = g B \quad (6)$$

where g is the gyromagnetic ratio of the particle and B is the static magnetic field. Since the spins each experience a slightly different magnetic field, they will precess at slightly different Larmour frequencies. Gradually, they will become out of phase with each other. The characteristic time for this dephasing is called T_2 or the spin relaxation time and is quantified as

$$M_{xy}(t) = M_{xy0} \exp(- t / T_2) \quad (7)$$

where $M_{xy}(t)$ is the net magnetization in the x-y plane as a function of time.

Spin-echo techniques take advantage of this dephasing. The three steps to a basic spin-echo NMR measurement are: 1. Apply a $\pi/2$ pulse, which rotates M from the z-axis to the x-y plane; 2. Wait for the spins to begin dephasing and recovering; 3. Apply a π pulse, which flips M to the other side of the x-y plane and partially rephases the spins, producing an echo, which appears as a pulse on the output. Diffusion measurements use a magnetic field gradient parallel to the static field (along the z-axis) that is pulsed on before and after the π pulse. This gradient dephases the spins that have moved out of a certain region, reducing their contribution to the echo. In this way, the time evolution of the echo amplitude indicates the rate at which the particles of interest move out of a region and thermalized particles move into the region.

This spin-echo technique has been used for studying ^{3}He diffusion in solid ^{4}He for rates down to 10^{-8} cm^2/s (Grigor'ev[6] and Richards *et al*[12]). The expression which relates the amplitude of the echo to the diffusion constant is

$$h = h_0 \exp[- 2 t / T_2 - (2/3) g^2 G^2 D t^3] \quad (8)$$

where h is the echo amplitude, t is the time interval between the $\pi/2$ and π pulses, g is the gyromagnetic ratio of ^{3}He (2.04×10^8 T^{-1}s^{-1}), G is the magnetic field gradient, and h_0 is the amplitude of the signal after the $\pi/2$ pulse.

At lower diffusion rates ($D < 10^{-8}$ cm^2/s), the spin-echo technique has too low of a signal-to-noise ratio. A stimulated echo technique, with three $\pi/2$ pulses, is used instead (Schratter *et al*[13]). The height of the stimulated echo is related to the diffusion constant through

$$h = h_0/2 \cdot \exp[-2t_1/T_2 - (t_2 - t_1)/T_1 - g^2 D t_1^2 (t_2 - t_1/3)] \quad (9)$$

where t_1 and t_2 are the intervals between the first and second pulses and the second and third pulses.

It is important to note that these NMR measurements correspond to the spin diffusion coefficient, which may differ from the ^{3}He diffusion coefficient if a method of spin transfer without displacement is available. Such methods involve spin-spin interactions and would only occur when other ^{3}He atoms are in close proximity. Thus, the measured diffusion coefficients may be attributed to the movement of actual atoms provided the fraction of ^{3}He is less than a few percent.

THE NEW TECHNIQUE

All previous measurements of isotopic impurity diffusion have assumed isotropic diffusion and only measured the diffusion coefficient in the direction of the static magnetic field. It is possible that impurity diffusion is more properly described by a tensor, rather than a constant. In order to measure more than one coefficient of the diffusion tensor, multiple gradients can be used. In the new technique, three orthogonal gradients are used: $\partial B_z/\partial z$, $\partial B_z/\partial y$, and $\partial B_z/\partial x$. The diffusion of ^{3}He is measured from the return of the spin system from a $\pi/2$ saturation and is quantified in

$$M_z(t) = M_0 \exp(-d^2 / D t G^2) \quad (10)$$

where d is the linewidth of the ^{3}He line (500 nT) and G is the field gradient (see the Appendix for a derivation of Equation 10).

With a gradient in the B_z field, the region that is in resonance with the $\pi/2$ pulse is only a narrow slice. The physical size of this slice depends on the linewidth of the ^{3}He resonance (d in Equation 10) and the field gradient (G). Only spins within the slice will become saturated, and the diffusion measured is for both the saturated spins leaving the gradient slice and thermalized spins entering.

This technique will only work if the diffusive transport of thermalized ^{3}He atoms into the region and of saturated atoms out increases M_z faster than the T_1 process (i.e. faster than the saturated ^{3}He atoms thermalize). For temperatures and pressures of interest, T_1 times are of order 100 s, and diffusion coefficients are of order 10^{-2}-10^{-8} cm^2/s (Schratter *et al*[13]). We must, therefore, apply a large enough field gradient to reduce the width of the slice w such that

$$t_D = w^2 / D < 100 \text{ s} \quad (11)$$

where t_D is the characteristic diffusion time. Creating a slice of width 10 μm would yield a diffusion time on the order of 100 μs, which is much less than 100 s, so the new technique is physically measurable.

To briefly summarize, the feature that makes this technique new is the use of three gradients. Using continuous-wave NMR rather than spin-echo techniques is done for simplicity, not because it is any better or worse.

APPARATUS

The apparatus consists of three parts: the NMR system, the cell in which the crystal is grown, and the refrigerator.

The NMR System

The functions of the NMR system are to establish the static magnetic field, to set up field gradients, to deliver the $\pi/2$ pulse, and to watch the system recover. To accomplish these tasks, we use various store-bought components and six of our own coils. All coils were wound with 0.0125 inch thick niobium tin superconducting wire, with the exception of the rf coil, whose wire was 0.0025 inches thick.

The static B_z field is set up by a 1 T superconducting magnet. We wound a solenoid so that we could compensate for any instability in the primary magnet's field without having to alter the current through it. This coil is 84.4 mm long and 41.7 mm in diameter with 268 turns.

The gradient of the magnetic field in the z direction (i.e. $\partial B_z/\partial z$) is set up by a Maxwell coil, which is a counter-wound Helmholtz coil. A diagram of the coil and a plot of its magnetic field is shown in Figure 3. The field along the z-axis of a Maxwell coil, with radius r, separation between the coils r, number of turns N, and current I is

$$B_z(z) = \frac{m_0 IN}{2r}\left\{\left[\left(\frac{z}{r}\right)^2 + \frac{z}{r} + \frac{5}{4}\right]^{-3/2} - \left[\left(\frac{z}{r}\right)^2 - \frac{z}{r} + \frac{5}{4}\right]^{-3/2}\right\} \quad (12)$$

Our coil has a diameter of 40 mm, a separation between the coils of half the diameter (the typical Helmholtz spacing), and 17 turns.

Gradients in the x and y directions are harder to make. The basic idea behind the coil we wound can be shown with four infinite wires carrying current in the same direction. With proper spacing, these wires can set up a gradient in the B_z field in the x or y direction (see Figure 4 for a diagram of the wires and a plot of the gradient field). If the current flows in the $-x$ direction, and the wires are separated by d in the y direction, and h in the z direction, and have current I flowing through them, then the field of the wires in the $x = 0$ plane is

$$B_z(y,z) = \frac{m_0 I}{2p}\left(\frac{\frac{d}{2}-y}{\left(\frac{d}{2}-y\right)^2+\left(\frac{h}{2}-z\right)^2} + \frac{\frac{d}{2}-y}{\left(\frac{d}{2}-y\right)^2+\left(-\frac{h}{2}-z\right)^2} + \frac{-\frac{d}{2}-y}{\left(-\frac{d}{2}-y\right)^2+\left(\frac{h}{2}-z\right)^2} + \frac{-\frac{d}{2}-y}{\left(-\frac{d}{2}-y\right)^2+\left(-\frac{h}{2}-z\right)^2}\right) \quad (13)$$

The coil design based on this gradient is called a Golay pair. Figure 5 shows a picture of a Golay pair, and a detailed calculation of the field produced by such a coil is carried out in Suits and Wilken[14] and Golay[15]. Note that the arc subtended by the wire is 120°, so the gap between opposite halves of the coil is 60°. We use two sets of Golay coils, one for $\partial B_z/\partial x$ and one for $\partial B_z/\partial y$. They have 13 turns each, a diameter of 48.5 mm, a separation between the upper and lower halves of (6.5 ± 5.0) mm, and a total length of (94 ± 5) mm. The reason for the uncertainty in separation and length is that the windings were wide. For example, the distance between the closest two wires of the upper and lower halves is 1.5 mm and between the farthest two is 11.5 mm, so we say that the halves are separated by (6.5 ± 5.0) mm.

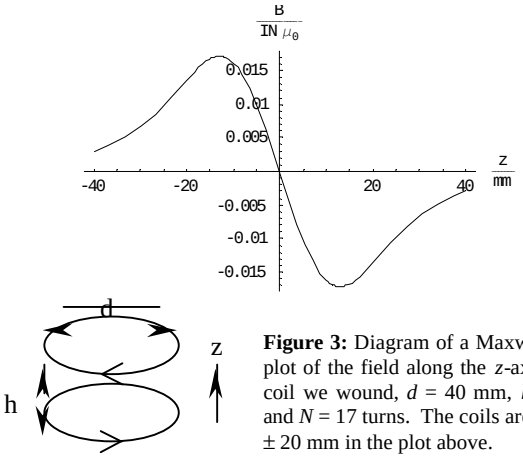

Figure 3: Diagram of a Maxwell coil and plot of the field along the z-axis. For the coil we wound, d = 40 mm, h = 20 mm, and N = 17 turns. The coils are at ± 20 mm in the plot above.

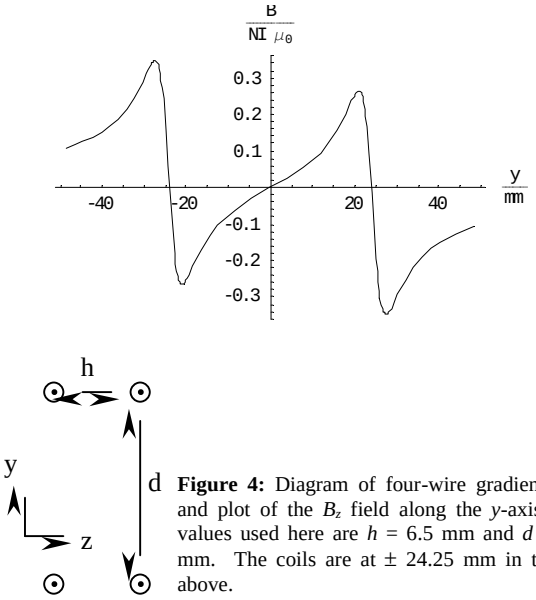

Figure 4: Diagram of four-wire gradient setup and plot of the B_z field along the y-axis. The values used here are h = 6.5 mm and d = 48.5 mm. The coils are at ± 24.25 mm in the plot above.

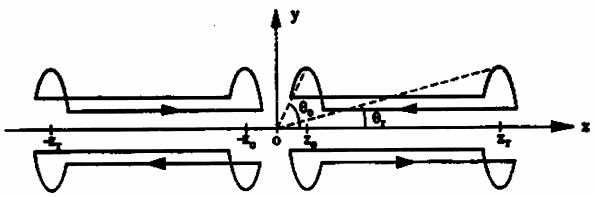

Figure 5: Picture of a Golay pair aligned to produce a gradient in the B_z field along the y-axis. For the coils we wound, z_0 = 3.25 mm, z_r = 47 mm, q_0 = 82°, and q_r = 27°. The arcs subtend an angle of 120°.

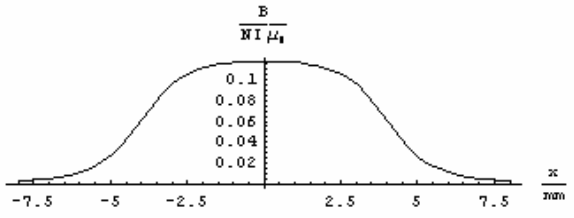

Figure 6: Plot of *B* field versus distance along the *x*-axis of the rf coil. The ends of the coil are at ± 4 mm, and the cell walls are at ± 6 mm. The field at the cell wall has dropped to 10% of its value at the center of the coil.

The coil used to deliver the π/2 pulse is a small solenoid (called the rf coil because it resonates at radio frequency). It is designed to fit inside the cell so that the helium grows around and through it. To aid this growth, slits were put in the coil-form. The coil is 8 mm long and 3 mm in diameter with 123 turns. Its magnetic field along the *z*-axis is plotted in Figure 6 and can be described with

$$B_z = \frac{m_0 IN}{2l}\left(\frac{\frac{l}{2}-z}{\sqrt{\left(\frac{l}{2}-z\right)^2+r^2}}+\frac{\frac{l}{2}+z}{\sqrt{\left(\frac{l}{2}+z\right)^2+r^2}}\right) \qquad (14)$$

The inductance of the rf coil can be calculated with

$$L = \alpha m_0 N^2 p\, r^2 / l \qquad (15)$$

and is 12.6 μH. Here, α is a fudge-factor so we do not overestimate the inductance; we used α = 0.75. The length-to-diameter ratio was important when designing the coil because we needed to create a uniform field along its axis, and we needed the field to drop rapidly outside the coil. Rapidly oscillating fields in the cell wall would induce eddy currents, which could alter field homogeneities and produce losses in the quality factor (*Q*) of the coil.

The sixth and final coil we wound was a modulation solenoid. Its purpose is to modulate the signal so that we can use a lock-in amplifier for detection. The solenoid is 95 mm long and 44 mm in diameter with 81 turns. When off, the resonant slice sits in the rf coil, which picks up the saturated spin signal. When on, it shifts the B_z field, moving the resonant slice outside of the rf coil, which no longer receives any signal.

We wound all of our coils on delcron (a plastic), with the exception of the rf coil, which was wound on teflon. We held the wires in place with GE varnish. The rf coil is mounted in the cell. The remaining coils are wound around coaxial cylinders that fit together around the cell and within the primary magnet.

We use a 50 Ω coaxial cable terminated in a 50 Ω resistor in parallel with the rf coil and a capacitor. The ratio of reflected to incident voltage is given by

$$V_{ref} / V_{inc} = (Z - 50) / (Z + 50) \qquad (16)$$

where *Z* is the impedance of the 50 Ω resistor and the LC circuit. The reflected power is zero at the coil resonance except when the rf power is absorbed by the spins.

A diagram of the NMR system appears in Figure 7. The attenuators, splitter, amplifier (with its power supply), rf switch, mixer, and transformer were mounted on a board, which will be attached to the refrigerator's support frame. A brief description of how to operate the NMR system appears in the Procedure section.

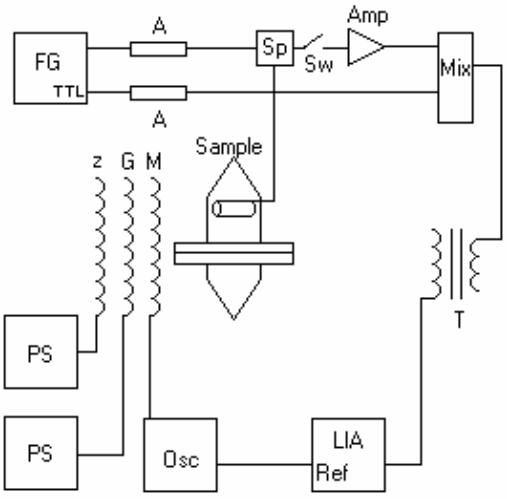

Figure 7: Diagram of the NMR system. The static magnetic field is established by the superconducting magnet (z) and the gradient coil (G). Each is run by its own power supply (PS). The saturating pulse is applied to the sample via a function generator (FG) through a splitter (Sp). The recovery signal returns to the splitter and goes through an amplifier (Amp). It enters the mixer (Mix) with a TTL signal from the function generator. The signal then gets stepped up in a transformer (T) and enters a lock-in amplifier (LIA). The signal is modulated with the modulation coil (M), which is driven by an oscillator (Osc) that also provides the LIA's reference signal. Two attenuators (A) on the lines prevent the signal from reflecting back to the function generator. An rf switch (Sw) opens during the pulses to prevent saturation of the amplifier and damage to the mixer.

The Cell

A sketch of the cell in which the helium will be frozen appears in Figure 8. It is made of non-magnetic stainless steel and holds roughly 1 cm^3 of helium when full. It has a cylindrical body with two conic ends and is split in half. The two halves are attached with a number of screws. The helium enters the cell through a capillary in the upper cone. The top of the cell will be slightly heated by several turns of wire so that a temperature gradient will form in it and the helium crystal will grow from the bottom to the top. The lower cone has a tiny piece of graphite (grafoil to be precise) in an effort to get the normal to the basal plane of the helium lattice oriented in the *z*–direction. The upper cone allows for the helium crystal to grow all the way to the top without leaving any pockets of liquid in corners (as could happen in a cylindrical cell).

The rf coil is mounted inside the cell on wooden "stilts" and is held in place with GE varnish. Two slots in

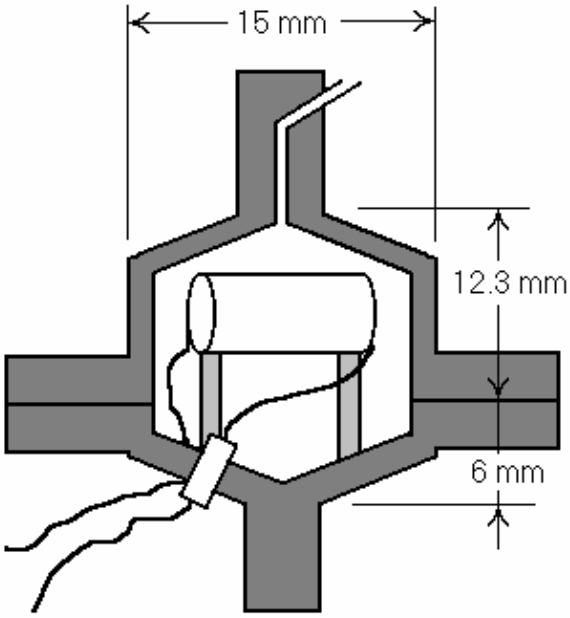

Figure 8: Diagram of the cell with dimensions (not to scale). The rf coil is mounted on two wooden stilts and electrically connected via a coax cable mounted in the cell wall. The helium is delivered through a capillary in the upper cone, and the crystal grows from the bottom up.

the coil form were designed to allow the crystal to grow through our coil windings to keep the orientation of the crystal. If the crystal grew from the ends with liquid trapped in the coil, the crystal would be highly strained. A coax cable comes through the lower cone of the cell to connect to the rf coil. The cable is sealed with epoxy so that the cell does not leak. One lead of the rf coil is connected to the wall of the cell (i.e. to ground) with silver paint. The other is connected to the center lead of the coax. Niobium tin wire cannot be soldered, so we wrapped the copper lead from the coax around the NbSn wire and soldered the copper to itself (effectively trapping the superconducting wire inside).

The Refrigerator

The refrigerator to be used works on pumped helium. It has two pots; one is for ^{4}He and the other for ^{3}He. When pumping on the ^{4}He pot, the temperature can reach 1.2 K. When pumping on the ^{3}He pot, the temperature can reach 0.25 K.

PROCEDURE

The procedure used to conduct this experiment can be broken into preliminary and operating phases. As this paper is being submitted, we are nearing completion of the preliminary phase.

The preliminary phase consists of the design and construction of the apparatus and the testing of the various systems. First, we designed the cell and the coil forms. As these designs were sent to the machine shop, we checked the thermal and electrical properties of several types of coax leads to see which would be optimal for taking power into the refrigerator to our coils. By dipping the leads in liquid helium and measuring the volume of helium boiled off due both to thermal conduction and to sending one amp through them, we determined that stainless steel coax with a copperweld inner conductor thermally conducted less heat into the helium than copper leads and heated to roughly the same temperature as copper when one amp was run through them. Thus, we decided to use the stainless steel leads.

When the coil forms returned from the machine shop, we began winding coils. The most difficult to wind were the Golay pairs because they required making spooled wire conform to a shape that alternated between curved and straight sections. Much time was spent waiting for the GE varnish to stick the corners down wherever the wire bent. When the coils were wound, connectors were soldered to their ends so that they could attach to the leads.

The refrigerator was modified for this experiment by adding new leads down the side and by redesigning a mounting plate for the cell. The leads were attached to a new face plate with BNC connectors and were run down the length of the fridge. They were heat sunk to the radiation shields in the dewar with copper plates. Connectors matching those on the coils were attached to their ends. The upper half of the cell was mounted on the ^{3}He pot.

After mounting the rf coil in the lower half of the cell, we checked its resonance (with the appropriate capacitor) to make sure that it was at 28 MHz. Figure 9 shows a diagram of the setup used to check the resonance. As frequency is swept upwards, the signal on the oscilloscope will rise, peak, and decline. The signal will be low below resonance because the inductor shorts it to ground. It will be low above resonance because the capacitor shorts it to ground. At resonance, however, the LC circuit has near-infinite impedance, so the signal will all go to the oscilloscope. Figure 10 shows the plot of voltage versus frequency that was obtained, indicating that there was some additional capacitance or inductance in the circuit that was shifting the resonant frequency down over 20 MHz. The rf coil had a calculated inductance of 12.6 μH and the capacitance in parallel was 3.2 pF, so there was an additional 50 pF somewhere in the circuit. Shortening the cables shifted the frequency somewhat. Changing the value of the resistance in the circuit did not shift the resonant frequency, indicating that the connecting cables did not have the dominant effect. After some time, we determined that it was the

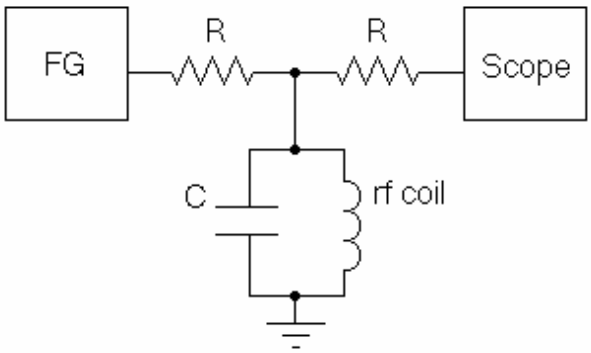

Figure 9: Diagram of the setup used to check the resonance of the rf coil. The function generator (FG) is swept through frequencies. Below and above the resonance of the LC circuit, the signal is shorted to ground; at the resonance, the impedance of the LC circuit is maximized, and the signal is transmitted. An oscilloscope (Scope) is used to monitor the signal.

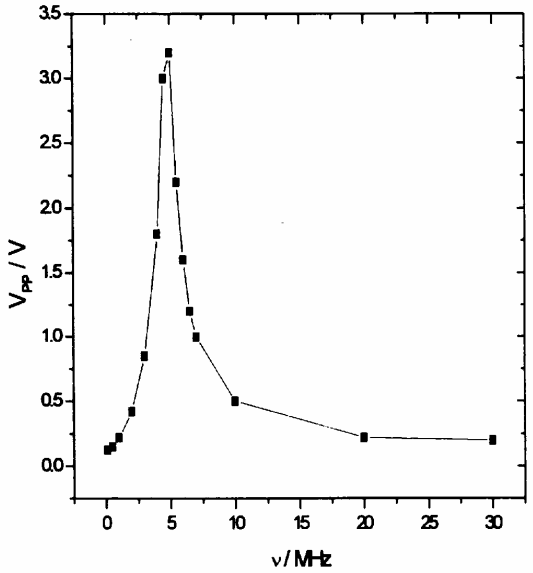

Figure 10: Plot of peak-to-peak voltage at the oscilloscope in Figure 10 versus frequency. Note the clear resonance at 5.5 MHz. This is far below the expected resonance at 28 MHz, indicating some unexpected capacitance in the system.

capacitance between adjacent windings in the coil that was contributing to our shifted resonance. We noted that in a similar apparatus used by Miyoshi *et al*[16], there were 50 turns in half of an inch, whereas we had 123 turns in 8 mm (over four times more dense). We are currently winding a second rf coil with half as many turns to see if the reduced inter-turn capacitance will bring the resonance back towards 28 MHz.

After the resonance of the saturation circuit is determined, we will cool down the system (so the wires will superconduct) and perform NMR on a piece of teflon. This run will serve two purposes: first, it will verify that the NMR system is operational, and second, it will act as a proof-of-concept for the tri-gradient and spectrometer-bridge methods.

Once the method has been demonstrated to work, we must make a relative calibration of the three gradient coils. For the calibration, we will use a dilute ^{3}He-^{4}He solution in either liquid helium or bcc ^{4}He, both of which are anticipated to have isotropic diffusion rates.

After calibration, we can begin to make runs on hcp helium. The basic procedure for these runs will be as follows. After being evacuated, the cell will be filled with 1 atm of ^{3}He gas. The refrigerator will be cooled, condensing the helium. The cell will then be filled with ^{4}He, which is pre-pressurized to 140 atm in a standard ^{4}He tank. A pressure regulator will allow the pressure to build to approximately 25 atm in the cell, and the helium will crystallize. Beginning with 1 atm of ^{3}He at room temperature yields a solid that is 0.1% ^{3}He. Since density of an ideal gas is inversely proportional to temperature, we can control the initial density of ^{3}He (and thus the final percentage) by varying the temperature at which it is admitted. Cooling the cell before adding the ^{3}He will produce a greater ^{3}He / ^{4}He ratio.

Once the sample is prepared, we will establish a magnetic field gradient in one direction, saturate the spins, and watch as they recover. As they recover, we will use a square-wave modulation to shift the resonant gradient slice during half the cycle. The spins will be given a π pulse during a half cycle of the modulation signal (the rf switch between the splitter and the amplifier will be opened during this pulse to prevent saturation of the amplifier and damage to the mixer). After the pulse, the resonant slice will be shifted out of the saturated part of the sample to another part of the sample (or perhaps out of the sample). The absorption will be different on the two halves of the modulation period, so a lock-in amplifier can be used. We will then switch to a second gradient, saturate, and watch as the spins recover. Finally, we will switch to the third gradient, saturate, and watch them recover. The diffusion constants from each of the gradients can be compared because we have calibrated the coils and because all measurements are being performed on the same single crystal. Differences in coil design, imperfections in winding, and strength of signal are not important to the measurement because we are making a relative time measurement not a precision amplitude measurement. That is, we are only looking for a difference in diffusion rates.

CONCLUSIONS

We sought out to study the motion, via tunneling into vacancies, of ^{3}He impurities in an hcp ^{4}He lattice. We have proposed a new technique, based on three orthogonal gradients, to look for anisotropies in this

tunneling rate and have built an apparatus to carry out this search. The experiment is near ready to begin operation.

ACKNOWLEDGEMENTS

I thank Professor Arnold Dahm for his guidance, enthusiasm, and willingness to share his expertise in this field. He has made this project an incredible learning experience. In addition, I thank Professor Robert Brown and Christopher Sica for their help with the NMR aspect of the project.

APPENDIX

To derive Equation 10, we begin with the diffusion equation:

$$J_n = - D \nabla n$$

where J_n is the number flux density, D is the diffusion coefficient, and n is the number density. We assume that the diffusion is in the z-direction and rewrite the above equation as

$$\frac{\partial}{\partial t}\left(\frac{N}{A}\right) = -D \frac{\partial}{\partial z}\left(\frac{N}{V}\right)$$

where A and V are some area and volume of interest. Integrating by t, we get

$$\frac{NV}{A} = -D \frac{\partial N}{\partial z} t$$

or

$$\frac{-V}{ADt} \int dz = \int \frac{dN}{N}$$

Integrating and assuming that $V = A\, z$, we get

$$N = N_0 \exp(-z^2 / D\, t)$$

Now, we consider a gradient

$$G = \frac{\partial B}{\partial z}$$

If the linewidth of the NMR resonance is d, the thickness of the slice is

$$z = \frac{d}{G}$$

Plugging into our equation for N and noting that the magnetism M is proportional to N, we arrive at Equation 10

$$M_z(t) = M_0 \exp(-d^2 / D\, t\, G^2)$$

REFERENCES

[1] K.H. Bennemann and J.B. Ketterson, The Physics of Liquid and Solid Helium, Part I, (New York: John Wiley & Sons, 1976), Ch. 6.
[2] H.R. Glyde, Excitations in Liquid and Solid Helium, (Oxford: Clarendon Press, 1994), Ch. 3.
[3] A.F. Andreev and I.M. Lifshitz, Zh. Eksp. Teor. Fiz. **56**, 2057 (1969) [Sov. Phys. JETP **29**, 1107 (1969)].
[4] A.R. Allen and M.G. Richards, Phys.Lett. **A65**, 36 (1978).
[5] A.R. Allen, M.G. Richards, and J. Schratter, J. Low Temp. Phys. **47**, 289 (1982).
[6] V.N. Grigor'ev, Fiz. Nizk. Temp. **23**, 5 (1997) [Low Temp. Phys. **23** (1), 3 (1997)].
[7] R.O. Simmons, J. Phys. Chem. Solids **55**, 895 (1994).
[8] S.C. Lau and A.J. Dahm, J. Low Temp. Phys. **112**, 47 (1998).
[9] S.C. Lau, W.J. Jeffers, Jr., and A.J. Dahm, J. Physique **39**, C6-86 (1978).
[10] O.A. Andreeva, K.O. Keshishev, and D.I. Kholin, JETP Lett. **65**, 95 (1978).
[11] O.A. Andreeve and K.O. Keshishev, private communication with A.J. Dahm.
[12] M.G. Richards, J. Pope, P.S. Tofts, and J.H. Smith, J. Low Temp. Phys. **24**, 1 (1976).
[13] J. Schratter, A.R. Allen, and M.G. Richards, J. Low Temp. Phys. **57**, 179 (1984).
[14] B.H. Suits and D.E. Wilken, J. Phys. E: Sci. Instrum. **22**, 565 (1989).
[15] M.J.E. Golay, Rev. Sci. Instrum. **29**, 313 (1958).
[16] D.S. Miyoshi, R.M. Cotts, A.S. Greenberg, and R.C. Richardson, Phys. Rev. A **2**, 870 (1970).